ACS APPLIED NANO MATERIALS

www.acsanm.org

Forum Article

Interferometric Phase Intensity Nanoscopy (iPINE), Revealing Nanostructural Features, Resolves Proximal Nanometer Objects below the Diffraction Limit: Implications in Long-Time Super-Resolution of Biological Dynamics

Guangjie Cui,[†] Do Young Kim,[†] Di Zu, Guanbo Chai, and Somin Eunice Lee*

Cite This: https://doi.org/10.1021/acsanm.3c04361

Read Online

ACCESS | Metrics & More | Article Recommendations | Supporting Information

ABSTRACT: The ability to spatially and temporally map nanoscale environments in situ over extended time scales would be transformative for biology, biomedicine, and bioengineering. All nanometer objects, from nanoparticles down to single proteins, scatter light. Interferometric scattering stands as a powerful tool, offering ultrasensitivity and resolution vital for visualizing nanoscale entities. Interferometric scattering from an individual nanoparticle down to an individual protein has been detected; however, resolving adjacent nanometer objects with interferometric scattering has not yet been demonstrated. In this work, we present interferometric phase intensity nanoscopy (iPINE) to resolve adjacent nanometer objects with interferometric scattering. We demonstrate that multiphase and sensitivity of iPINE reveal ellipse Airy patterns correlated with nanostructural features. We show that eliminating background fluctuation by employing circularly polarized illumination in iPINE is essential to separate proximal nanometer objects below the diffraction limit. We envision iPINE for resolving a variety of adjacent nanometer objects from nanoparticles down to proximal proteins in situ over extended time periods for a wide range of applications in biology, biomedicine, and bioengineering. We expect iPINE to be especially important in applications of biological dynamics that require extended observation times.

KEYWORDS: *plasmonic super-resolution, scattering super-resolution, bioplasmonics, long-term nanoscopy, interferometric scattering*

INTRODUCTION

Mapping the temporal (dynamic) heterogeneity of nano-environments (Figure 1a) is critical to designing new smart materials and precision therapeutics, but broad time scales constrain time-resolved efforts at the expense of spatial resolution.[1−4] All nanometer objects, from nanoparticles down to single proteins, scatter light. Recently interferometric scattering has become a tremendously powerful optical imaging method with sensitivities capable of observing scattering from individual nanometer objects.[5−16] Due to the principle of interference, where the superposition of light waves can amplify or diminish their resultant intensity, interferometric scattering microscopy (iSCAT) detects the first order interference term rather than the quadratic scattering component, enabling detection of an individual nanoparticle and individual virus and even an individual lipid and individual protein. As iSCAT utilizes scattering from the target, iSCAT is able to bypass photobleaching and phototoxicity problems occurring over extended time periods, currently hampering traditional fluorescence microscopy.

To date, interferometric scattering from an individual nanoparticle down to an individual protein has been detected;[5,6] however, resolving adjacent nanometer objects in a diffraction limited region with interferometric scattering has not yet been demonstrated. While the localization of an individual nanometer object using interferometric scattering is well established, resolving adjacent targets with interferometric scattering remains challenging. This is due in part because in coherent imaging scattering light from adjacent targets no longer comes from the addition of intensity but the superposition of the amplitude and phase of each electromagnetic field.

Here, we overcome these challenges by interferometric phase intensity nanoscopy (iPINE). By integrating a phase-intensity multilayer thin film,[17] herein referred to as PI, with interferometric scattering, nanometer objects below the diffraction limit can be resolved. While coherent imaging superimposes amplitude and phase of electromagnetic fields, phase-intensity modulation in iPINE enables one to separate the intensity and phase such that nanometer objects are distinguished at different phases and adjacent targets can be then resolved. We have established that multiphase analysis and sensitivity of iPINE bring to light ellipse Airy patterns that correlate with nanostructural characteristics. Our results also indicate that the use of circularly polarized illumination in iPINE is essential to break the diffraction threshold in differentiating between proximal nanometer objects. iPINE is

Special Issue: Women in Nano

Received: September 13, 2023
Revised: January 14, 2024
Accepted: January 16, 2024

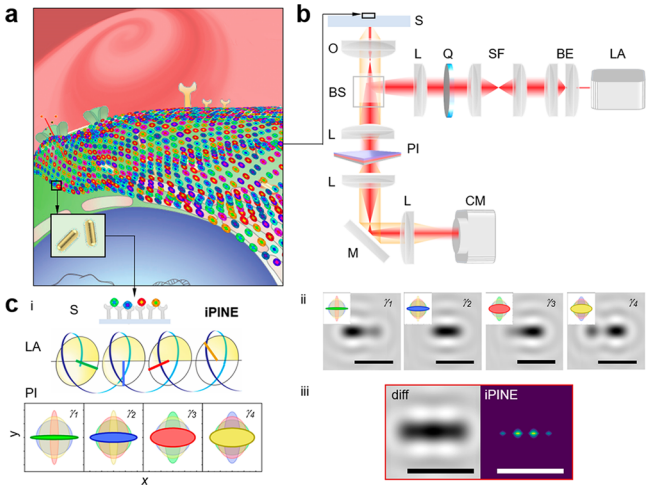

Figure 1. Interferometric phase intensity nanoscopy (iPINE)—revealing nanostructural features—resolves adjacent nanometer objects below the diffraction limit. (a) All nanometer objects, from nanoparticles down to single proteins, scatter light. In this work, adjacent nanometer objects, gold nanorods (Au), are resolved by interferometric phase intensity nanoscopy (iPINE). We envision resolving adjacent proteins in living cells by iPINE in the future. (b) Experimental setup of the iPINE: PI device, consisting of a fixed quarter wave retarding polymer element, a variable full wave retarding polymer element, and a fixed linear polarizing polymer element, was integrated into the detection path of an interferometric scattering microscope to achieve phase modulation. In order to eliminate signal-to-noise fluctuation and detector saturation during phase modulation, quarter waveplate (Q) was inserted in the illumination path in order to convert the illumination source (LA) from linear to circular. S: sample, O: objective, L: lens, SF: spatial filter, BE: beam expansion lenses, M: mirror, CM: CMOS camera. (c) Principle of iPINE: (i) iPINE resolves adjacent nanometer objects (green, blue, red, orange) below the diffraction limit. Nanometer objects are illuminated by circularly polarized light (LA). After phase modulation of γ (PI), nanometer objects, diverse in their phases, exhibit different scattering electric fields. (ii) Representative interferometric images ($\gamma_1 = 0.41\pi$ rad, $\gamma_2 = 0.88\pi$ rad, $\gamma_3 = 1.12\pi$ rad, $\gamma_4 = 1.82\pi$ rad) over the phase modulation range. (iii) Diffraction-limited interferometric scattering image. iPINE-resolved image. Scale bar: 500 nm.

particularly useful in biological applications where extended time scales cannot be reached using traditional fluorescence methods. We envision iPINE can resolve a variety of nanometer objects, from nanoparticles down to proteins, in the future in order to map spatial and temporal (dynamic) heterogeneity of nanoenvironments in situ over extended time scales in biology, biomedicine, and bioengineering.

RESULTS

Interferometric scattering from an individual nanoparticle down to an individual protein has been detected; however, resolving adjacent nanometer objects with interferometric scattering has not yet been demonstrated. We resolve adjacent nanometer objects with interferometric scattering by interferometric phase intensity nanoscopy. iPINE provides outstanding sensitivity beyond traditional interferometric scattering microscopy by remapping the target's phase into intensity to reveal nanostructural details and resolve adjacent nanometer objects. iPINE detects the difference between a reference field and the modulated sample scattered field.

$$I = |E_r + (E_S, \gamma)|^2 \approx |E_r|^2 - 2|E_r||(E_S, \gamma)|\cos\phi \quad (1)$$

where I is the intensity, E_r is the reference field, $\mathcal{P}(E_S, \gamma)$ represents the modulated scattered field by PI, and ϕ denotes the relative phase between nanoprobes and reference plane irrelevant from modulation. The PI device in iPINE plays an important role in modulating the intensity of scattered field:

$$\begin{aligned} |\mathcal{P}(E_S, \gamma)| &= \left| \begin{bmatrix} 1 & 0 \\ 0 & 0 \end{bmatrix} \frac{1}{2} \begin{bmatrix} e^{i\gamma/2} + e^{-i\gamma/2} & e^{i\gamma/2} - e^{-i\gamma/2} \\ e^{i\gamma/2} - e^{-i\gamma/2} & e^{i\gamma/2} + e^{-i\gamma/2} \end{bmatrix} \right. \\ &\quad \left. e^{i\pi/4} \begin{bmatrix} 1 & 0 \\ 0 & -i \end{bmatrix} [E_S^x E_S^y] \right| \\ &= \left| \cos\frac{\gamma}{2} E_S^x + \sin\frac{\gamma}{2} E_S^y \right| \end{aligned} \quad (2)$$

where the terms of the Jones matrices represent a fixed quarter wave retarding element, variable full wave retarding element, and a fixed linear polarizing element of PI.[17] When the scattered light propagates through PI with phase retardation γ, the modulation of the contrast is characterized as

$$C_{iPINE} = \frac{4|\mathcal{P}(E_S)|}{|E_r|}\cos\phi \quad (3)$$

To implement iPINE, we integrated PI into the detection path of an interferometric scattering microscope to achieve phase modulation (Figure 1b). Illumination laser (710 nm) was followed by a spatial filter and beam expansion optics to improve beam quality. In this work, we report that eliminating background fluctuation by employing circularly polarized illumination in iPINE is necessary to separate adjacent nanometer objects below the diffraction limit. To convert the illumination source from linear to circular, a quarter waveplate was inserted in the illumination path in order to eliminate signal-to-noise fluctuation and detector saturation during phase modulation. The major noise then is the shot noise which decreases with the increasing number of photons N collected by the detector during the exposure time. Thus, the reference light amplitude remains constant to guarantee a high signal-to-noise ratio as well as to avoid signal-to-noise fluctuation and detector saturation.

$$\frac{d||\mathcal{P}(E_r, \gamma)|}{d\gamma} = \frac{\frac{1}{2}d|E_r|}{d\gamma} = 0 \quad (4)$$

After reflection on a beam splitter, the beam was focused on the back focal plane of the objective lens, creating a wide-field planar illumination on the sample. Both scattered light and reference beam were collected by the high numerical aperture oil-immersed objective lens and propagated through PI, converting the phase to intensity modulation. This phase to intensity modulation distinguishes iPINE from traditional iSCAT to resolve adjacent nanoprobes below the diffraction limit. As an example, four adjacent nanometer objects were indistinguishable in the diffraction limited interferometric scattering image (Figure 1c). Unlike iSCAT which only considers the intensity, iPINE offers multiphase and sensitivity to reveal anisotropic Airy patterns correlated with nanostructural features. By employing modulation of different phases, iPINE resolves adjacent nanometer objects below the diffraction limit (Figure 1c).

Notably, we observed elliptical Airy patterns by iPINE which were not previously reported in traditional iSCAT.[14,18] We

https://doi.org/10.1021/acsanm.3c04361
ACS Appl. Nano Mater. XXXX, XXX, XXX−XXX

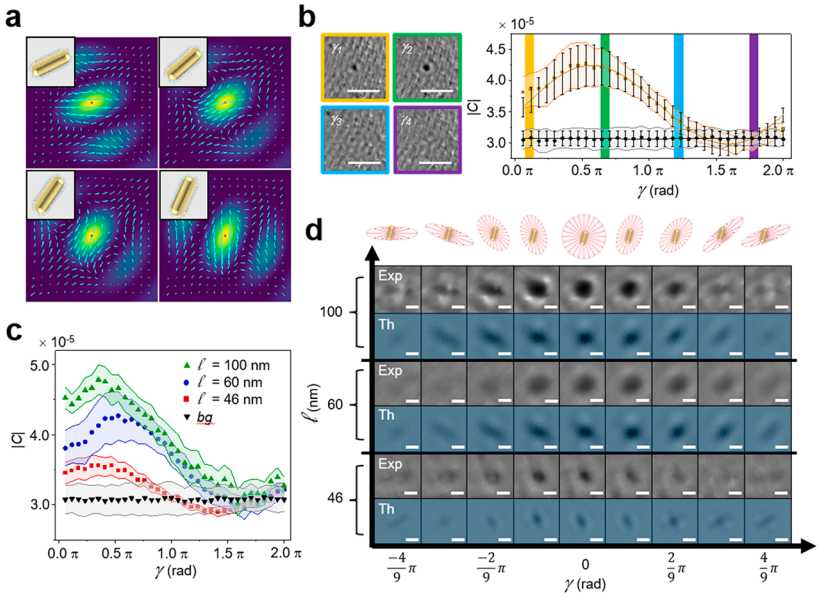

Figure 2. Multiphase and sensitivity of iPINE reveals ellipse Airy patterns correlated to nanostructural features. (a) Nanostructural feature (dipole moment): Far field radiation patterns, electric field vector plot (cyan arrows) overlaid with the intensity pattern (color map) representing the varying nanostructural feature (dipole moment) of the model nanometer object (gold nanorod). (b) Owing to phase-intensity modulation, iPINE distinguished the target that was hidden by the background noise. Representative interferometric images: $\gamma_1 = 0.1\pi$ rad (yellow shading), $\gamma_2 = 0.7\pi$ rad (green shading), $\gamma_3 = 1.2\pi$ rad (blue shading), $\gamma_4 = 1.8\pi$ rad (purple shading). Scale bar: 1 μm. Graph of absolute contrast |C| versus phase γ for model nanometer object (gold nanorod), gold line and background noise, black line. (c) Graph of absolute contrast |C| versus phase γ as a function of nanometer object size. (d) iPINE reveals ellipse Airy patterns: Theoretical (Th) and experimental (Exp) interferometric scattering results over the phase modulation range γ with respect to size. Scale bar: 200 nm.

hypothesized that elliptical Airy patterns originate from the anisotropic nanostructural features of the target. The size of the elliptical Airy pattern would be limited by the diffraction limit; however, we anticipate that the ellipticity and the intensity of the elliptical Airy pattern would vary due to the dependence between the scattered field amplitude and the scattering cross-section of the target. As a model candidate of an anisotropic[19−53] nanostructured target to validate the fundamental reason that we can see the ellipse Airy pattern, we simulated the scattered electric field pattern of gold nanorods (Figure 2a). Here, we acquired the nanostructural information from the ellipse Airy pattern by phase-intensity and phase-ellipticity. The phase-intensity reveals the eclipsed information (Figure 2b) from the background noise. Traditional iSCAT relies on differential images with and without the target of interest in order to reduce the background noise. However, iPINE can detect the target, which was initially covered by the background noise owing to the phase-intensity modulation. Figure 2b shows the detection of the target hidden by background noise. The target cannot be detected at γ denoted by the purple shading because the contrast of the target (gold nanorod; gold line) overlaps with the background noise (black line). On the other hand, at γ denoted by the green shading, the contrast of target (gold nanorod, gold line) is significantly higher than the background (black line). Owing to the dependence between the scattered electric field and the scattering cross-section, the target's detectable phase range also varies. We varied the target size and observed larger targets show a higher contrast, allowing for a larger range of phase distribution and more ellipticity variation. (Figure 2c) Furthermore, not only was more data collected, but iPINE also acquired more nanostructural information than traditional iSCAT.[14] The simulation of the phase-intensity with the phase-ellipticity demonstrates the trend to the elliptical Airy pattern of each specific phase by PI. The scattered electric field vector finally makes some rotation and the reduction of the amplitude (Supplementary Figures S1 and S2), which leads to ellipticity variation with the rotation of gold nanorods (Supplementary Figure S3).

$$I_{det} = \cos^2\frac{\gamma}{2}|E_{r_x}|^2 + \cos^2\left(\frac{\gamma}{2} - \theta_p\right)|E_{s_x}|^2 + 2\cos\left(\frac{\gamma}{2} - \theta_p\right)\cos\frac{\gamma}{2}|E_{r_x}||E_{s_x}|\cos\Delta\varphi_x + \sin^2\frac{\gamma}{2}|E_{r_y}|^2 + \sin^2\left(\frac{\gamma}{2} + \theta_p\right)|E_{s_y}|^2 + 2\sin\left(\frac{\gamma}{2} + \theta_p\right)\sin\frac{\gamma}{2}|E_{r_y}||E_{s_y}| \cos\Delta\varphi_y \quad (5)$$

where I_{det} is the intensity of the detector plane, $\frac{\gamma}{2}$ is the phase retardation through PI, θ_p is the major axis of gold nanorods from the x-axis, E_{r_x}, E_{r_y} are the x- and y-components of the reflected electric field from the glass slide, E_{s_x}, E_{s_y} are the x- and y-component of the scattered electric field from the gold nanorods, and $\Delta\varphi_x$, $\Delta\varphi_y$ are the phase different between scattered electric field and reflected electric field for each axis. The detector plane intensity is governed by the derived equation. Therefore, the exact rotation and variation of ellipticity can be ascertained by theoretical simulation, in agreement with experimental data (Figure 2d). We found the same patterns with diffraction limited size with varying intensity from different sizes and phases in both theoretical and experimental results. We also detected more dramatic changes of ellipticity with larger size of particles, showing a similar trend through the phase change. Control experiments, optical simulations, and numerical analysis were conducted to

https://doi.org/10.1021/acsanm.3c04361
ACS Appl. Nano Mater. XXXX, XXX, XXX−XXX

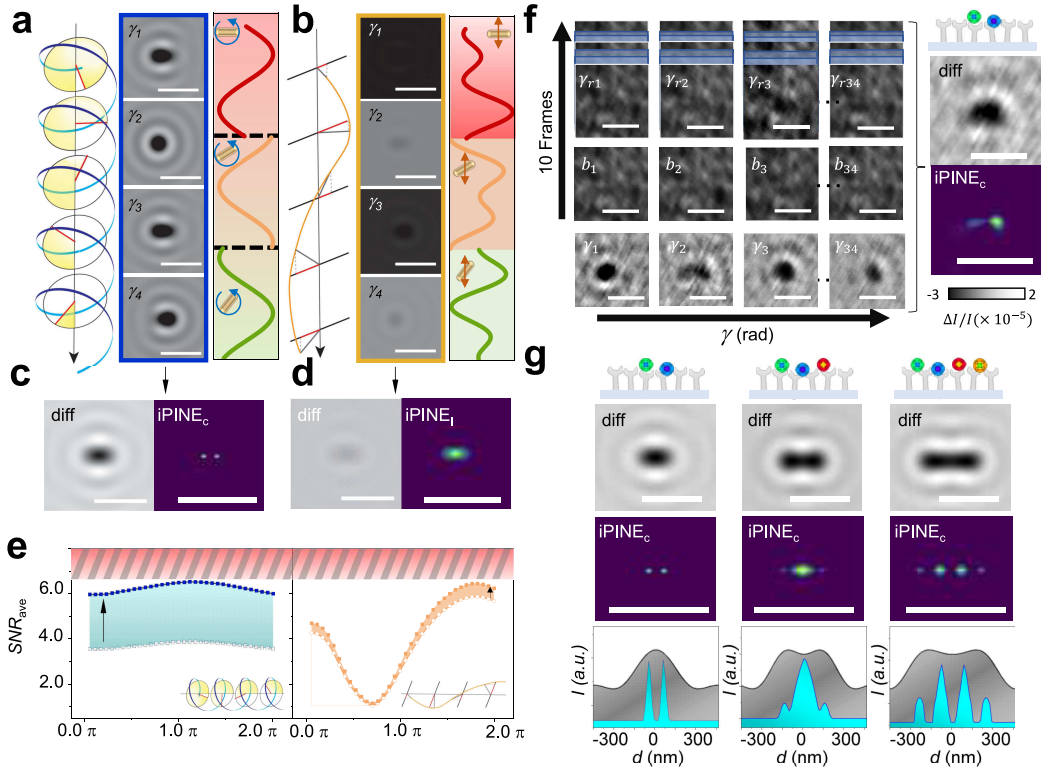

Figure 3. Eliminating background fluctuation by employing circularly polarized illumination in iPINE is necessary to separate adjacent nanometer objects below the diffraction limit. (a) Conceptual schematic of iPINE$_c$: (left) input to PI, circularly polarized illumination, (middle) simulated interferometric images over the phase modulation range γ from 0 to 2π, with an interval of 0.4π, (right) output after PI where green, orange, and red zones correspond to various dipole moments. (b) Conceptual schematic of iPINE$_l$: (left) input to PI, linearly polarized illumination, (middle) simulated interferometric images over the phase modulation range γ from 0 to 2π, with interval of 0.4π, (right) output after PI where green, orange, and red zones correspond to various dipole moments. (c) iPINE$_c$ is necessary to resolve proximal nanometer objects: iPINE$_c$: (left) diffraction-limited interferometric image, (right) iPINE$_c$-resolved image. (d) iPINE$_l$: (left) diffraction-limited interferometric image, (right) unresolved iPINE$_l$ image. Scale bar: 500 nm. (e) Average signal-to-noise ratio graph of circularly (left) and linearly (right) polarized illumination over the phase modulation range. The shadowed zone on the top part of the graph indicates the upper bound number of photons collected by detector. The circularly polarized light (blue curve) holds a higher place in the SNR plot than linearly polarized light (yellow curve) because more photons can be collected without saturation. Shot noise is considered here while the full well capacity of our sCMOS camera is 45 000 e^-. (f) iPINE$_c$ experimental procedure: Four out of thirty-four sets of images over the phase modulation range from 0 to 2π are shown. Target image is averaged from 10 frames under the same γ to repress noise. While background image is generated by applying median filter to images captured when the stage is modulated. (top) Diffraction limited interferometric image. (bottom) iPINE$_c$-resolved image. Scale bar: 500 nm. (g) iPINE$_c$ resolves multiple proximal nanometer objects: Simulation of two, three, and four proximal nanometer objects. The distance between the adjacent nanoprobes is 150 nm while the diffraction limit is 300 nm in setup. Diffraction-limited interferometric image, iPINE$_c$-resolved image. Scale bar = Scale bar: 500 nm. Intensity profile graphs plotted along line profiles in the corresponding diffraction limited interferometric image and iPINE$_c$-resolved image. blue color: iPINE$_c$-resolved. gray color: diffraction-limited.

exclude any other possibilities for elliptical airy patterns, such aberrations from the imaging system, polarization effects from the laser source, polarization purity, etc. (Supplementary Figures S6 and S7, Supplemental Notes II, III, IV). Thus, we can extract not only the phase information on nanometer objects but also employ modulation of ellipticity with different phases which can be applied to the iPINE for resolving adjacent nano-objects below the diffraction limit.

To resolve adjacent nanometer objects below the diffraction limit, we found that eliminating background fluctuation by employing circularly polarized illumination in iPINE was necessary to promote resolution. Circularly polarized illumination, as a key part in iPINE, provides constant-intensity reference field and enables efficient background elimination for high contrast (eq 3). To this end, we compared illumination sources: circularly polarized illumination as compared to linearly polarized illumination in iPINE. In Figure 3a, circularly polarized illumination provides an invariable background input that is correlated with nanostructural features (dipole moment), generating stable, in-phase contrast output over the phase modulation range. On the contrary, linearly polarized illumination caused the background to fluctuate over the phase modulation range as shown in the contrast images shown in Figure 3b, leading to low contrast in dark frames. In addition, the misalignment between the dipole moment with respect to linear polarization main axis distorts the phase of contrast output during modulation, lowering overall contrast and making subsequent loss of the ability to resolve adjacent nanometer objects (Figure 3c and d). In the experiment (Supplementary Figure S4), the stability of the background intensity as indicated in Figure 3e endorses the possibility to compensate for the intensity loss during modulation progress by increasing the overall illumination power or exposure time to catch up the upper-bound photon number limit which is usually determined by the detector's full well capacity or the sample's photodamage threshold. On the other hand as shown

https://doi.org/10.1021/acsanm.3c04361
ACS Appl. Nano Mater. XXXX, XXX, XXX−XXX

in Figure 3e, nanoprobes under linear polarization illumination are limited by the low signal-to-noise (SNR) dilemma: the dark retardation region ($\gamma \in [0.5\pi, 1.0\pi]$) with low SNR has redundancy in accommodating photons to reduce shot noise while higher photon flux vastly saturates the bright retardation region ($\gamma \in [0.5\pi, 2.0\pi]$). Here, we demonstrate that experimentally we can resolve adjacent nanometer objects. Figure 3f demonstrates the experiment of iPINE in resolving adjacent nanoprobes with an approximate distance of 190 nm (diffraction limit: 380 nm for coherent imaging). Supplementary Figure S5 shows that the minimum separation is currently 190 nm. In the future, the resolution of our setup could be further improved by taking the depolarization and phase retardation properties of nanoprobes into consideration. Images were captured over the phase modulation range, with images averaging at each γ to repress shot noise. To remove the unwanted speckles from the distortion of beam wavefront, we modulated the stage with a frequency of 17 Hz at 2 cm/s. Median background image was calculated from a bundle of background images under each γ. Adjacent nanometer objects were indistinguishable in the diffraction limited image, whereas adjacent nanometer objects were resolved in the iPINE image (Figure 3f). Furthermore, iPINE is not limited to the simple case of two nanoprobes. In Figure 3g, we extended the application of iPINE to multiple nanoprobes. Results show that iPINE can resolve multiple nanometer objects regardless of the more complicated interference introduced by the overlapping Airy patterns of adjacent nanoprobes (Figure 3g).

DISCUSSION

Despite gold nanorods possessing significantly greater polarizability than biological objects, iPINE can be also extended to proteins displaying anisotropic structural alterations.[54] The ribosome stands out as a prominent biological entity characterized by its anisotropic structure, showcasing anisotropic structural alterations in its translation mechanism.[55] Due to its anisotropic structural alterations, elliptical Airy patterns from ribosomes are realizable by iPINE. Because the scattered light is not governed by one single axis of polarization, scattered light from ribosomes shows different responses to phase retardation (proof of concept: Figure S8). Future work is underway to visualize anisotropic structural alterations with iPINE.

In this work, we demonstrate the breakthrough of the diffraction limit with iPINE enabled by phase intensity modulation with circularly polarized illumination. Some limitations in our current setup are nano-objects have different responses to the phase intensity modulation of iPINE. It is possible that other nanometer objects could reject scattering circularly polarized illumination light, making it difficult to detect and resolve them. As a solution, other modulation devices[42] could be inserted into the illumination optical path to replace the quarter waveplate enabling more complex modulation of the illumination source. Furthermore, iPINE could improve its sensitivity for wider applications by suppressing other noise, such as stemming from the detector, laser intensity fluctuations, and phase noises caused by vibrations, through optimized analysis methods.[56] Speckle-like background related shot noise can be reduced in the future by using self-supervised machine learning.[57] Future work is underway to enable iPINE to detect and resolve a wide variety of nanometer objects from nanoparticles to proteins.

CONCLUSION

In this paper, we report iPINE, which allows us to acquire nanostructural information from the ellipse Airy patterns and the varying phase intensity. Additionally, iPINE enables breaking the diffraction limit by mitigating the background fluctuation by PI, enabling sufficiently high contrast to address the nanoscale objects in close proximity. We anticipate that iPINE would play critical roles in long-time super-resolution applications, especially in applications with biological dynamics, which can reveal in situ observations over extended time periods in living cells down to single proteins in biology, biomedicine, and bioengineering.

ASSOCIATED CONTENT

Supporting Information

The Supporting Information is available free of charge at https://pubs.acs.org/doi/10.1021/acsanm.3c04361.

Materials, Methods, Supplemental Notes, Supplementary Figures, and Supplementary References (PDF)

AUTHOR INFORMATION

Corresponding Author

Somin Eunice Lee − *Department of Electrical & Computer Engineering, University of Michigan, Ann Arbor, Michigan 48109, United States; Department of Biomedical Engineering, Biointerfaces Institute, Applied Physics, and Macromolecular Science & Engineering, University of Michigan, Ann Arbor, Michigan 48109, United States;* orcid.org/0000-0002-6784-4043; Email: sleee@umich.edu

Authors

Guangjie Cui − *Department of Electrical & Computer Engineering, University of Michigan, Ann Arbor, Michigan 48109, United States*

Do Young Kim − *Department of Electrical & Computer Engineering, University of Michigan, Ann Arbor, Michigan 48109, United States*

Di Zu − *Department of Electrical & Computer Engineering, University of Michigan, Ann Arbor, Michigan 48109, United States*

Guanbo Chai − *Department of Electrical & Computer Engineering, University of Michigan, Ann Arbor, Michigan 48109, United States*

Complete contact information is available at: https://pubs.acs.org/10.1021/acsanm.3c04361

Author Contributions

†G.C. and D.Y.K. contributed equally.

Notes

The authors declare no competing financial interest.

ACKNOWLEDGMENTS

This work was supported by the Air Force Office of Scientific Research (AFOSR FA9550-19-1-0186, FA9550-22-1-0285, S.E.L.)

REFERENCES

(1) Karsenti, E. Self-Organization in Cell Biology: A Brief History. *Nat. Rev. Mol. Cell Biol.* **2008**, *9* (3), 255.

(2) Dawson, K. A.; Yan, Y. Current Understanding of Biological Identity at the Nanoscale and Future Prospects. *Nat. Nanotechnol* **2021**, *16* (3), 229−242.
(3) Ruiz-Rodado, V.; Lita, A.; Larion, M. Advances in Measuring Cancer Cell Metabolism with Subcellular Resolution. *Nat. Methods* **2022**, *19* (9), 1048−1063.
(4) Jerković, I.; Cavalli, G. Understanding 3D Genome Organization by Multidisciplinary Methods. *Nat. Rev. Mol. Cell Biol.* **2021**, *22* (8), 511−528.
(5) Piliarik, M.; Sandoghdar, V. Direct Optical Sensing of Single Unlabelled Proteins and Super-Resolution Imaging of Their Binding Sites. *Nat. Commun.* **2014**, *5*, 4495.
(6) Young, G.; Hundt, N.; Cole, D.; Fineberg, A.; Andrecka, J.; Tyler, A.; Olerinyova, A.; Ansari, A.; Marklund, E. G.; Collier, M. P.; et al. Quantitative Mass Imaging of Single Biological Macromolecules. *Science.* **2018**, *360*, 423−427.
(7) Kukura, P.; Ewers, H.; Müller, C.; Renn, A.; Helenius, A.; Sandoghdar, V. High-Speed Nanoscopic Tracking of the Position and Orientation of a Single Virus. *Nat. Methods* **2009**, *6* (12), 923−927.
(8) Spindler, S.; Sibold, J.; Gholami Mahmoodabadi, R.; Steinem, C.; Sandoghdar, V. High-Speed Microscopy of Diffusion in Pore-Spanning Lipid Membranes. *Nano Lett.* **2018**, *18* (8), 5262−5271.
(9) Taylor, R. W.; Mahmoodabadi, R. G.; Rauschenberger, V.; Giessl, A.; Schambony, A.; Sandoghdar, V. Interferometric Scattering Microscopy Reveals Microsecond Nanoscopic Protein Motion on a Live Cell Membrane. *Nat. Photonics* **2019**, *13* (7), 480−487.
(10) Cole, D.; Young, G.; Weigel, A.; Sebesta, A.; Kukura, P. Label-Free Single-Molecule Imaging with Numerical-Aperture-Shaped Interferometric Scattering Microscopy. *ACS Photonics* **2017**, *4* (2), 211−216.
(11) Ortega Arroyo, J.; Cole, D.; Kukura, P. Interferometric Scattering Microscopy and Its Combination with Single-Molecule Fluorescence Imaging. *Nat. Protoc* **2016**, *11* (4), 617−633.
(12) McDonald, M. P.; Gemeinhardt, A.; König, K.; Piliarik, M.; Schaffer, S.; Völkl, S.; Aigner, M.; Mackensen, A.; Sandoghdar, V. Visualizing Single-Cell Secretion Dynamics with Single-Protein Sensitivity. *Nano Lett.* **2018**, *18* (1), 513−519.
(13) Taylor, R. W.; Sandoghdar, V. Interferometric Scattering (ISCAT) Microscopy and Related Techniques. In *Label-Free Super-Resolution Microscopy*; Springer, 2019; pp 25−65.
(14) Lee, I. B.; Moon, H. M.; Joo, J. H.; Kim, K. H.; Hong, S. C.; Cho, M. Interferometric Scattering Microscopy with Polarization-Selective Dual Detection Scheme: Capturing the Orientational Information of Anisotropic Nanometric Objects. *ACS Photonics* **2018**, *5* (3), 797−804.
(15) Peeters, D. Interferometric Scattering Microscopy of Plasmonic Nanoparticles for Biosensing. *Masters Thesis*; Eindhoven University of Technology, Eindhoven, The Netherlands, 2022.
(16) Taylor, R. W.; Sandoghdar, V. Interferometric Scattering Microscopy: Seeing Single Nanoparticles and Molecules via Rayleigh Scattering. *Nano Lett.* **2019**, *19* (8), 4827−4835.
(17) Cui, G.; Liu, Y.; Zu, D.; Zhao, X.; Zhang, Z.; Kim, D. Y.; Senaratne, P.; Fox, A.; Sept, D.; Park, Y.; Lee, S. E. Phase Intensity Nanoscope (PINE) Opens Long-Time Investigation Windows of Living Matter. *Nat. Commun.* **2023**, *14* (1), 4318.
(18) Gholami Mahmoodabadi, R.; Taylor, R. W.; Kaller, M.; Spindler, S.; Mazaheri, M.; Kasaian, K.; Sandoghdar, V. Point Spread Function in Interferometric Scattering Microscopy (ISCAT). Part I: Aberrations in Defocusing and Axial Localization. *Opt Express* **2020**, *28* (18), 25969.
(19) Knight, M. W.; Liu, L.; Wang, Y.; Brown, L.; Mukherjee, S.; King, N. S.; Everitt, H. O.; Nordlander, P.; Halas, N. J. Aluminum Plasmonic Nanoantennas. *Nano Lett.* **2012**, *12* (11), 6000−6004.
(20) Perez-Juste, J.; Rodriguez-Gonzalez, B.; Mulvaney, P.; Liz-Marzan, L. M. Optical Control and Patterning of Gold-Nanorod-Poly(Vinyl Alcohol) Nanocomposite Films. *Adv. Funct Mater.* **2005**, *15* (7), 1065−1071.
(21) Huang, X.; El-Sayed, I. H.; Qian, W.; El-Sayed, M. A. Cancer Cells Assemble and Align Gold Nanorods Conjugated to Antibodies to Produce Highly Enhanced, Sharp, and Polarized Surface Raman Spectra: A Potential Cancer Diagnostic Marker. *Nano Lett.* **2007**, *7* (6), 1591−1597.
(22) Wang, G.; Sun, W.; Luo, Y.; Fang, N. Resolving Rotational Motions of Nano-Objects in Engineered Environments and Live Cells with Gold Nanorods and Differential Interference Contrast Microscopy. *J. Am. Chem. Soc.* **2010**, *132* (46), 16417−16422.
(23) Chang, W.-S.; Ha, J. W.; Slaughter, L. S.; Link, S. Plasmonic Nanorod Absorbers as Orientation Sensors. *Proc. Natl. Acad. Sci. U. S. A.* **2010**, *107* (7), 2781−2786.
(24) Nikoobakht, B.; El-Sayed, M. A. Preparation and Growth Mechanism of Gold Nanorods (NRs) Using Seed-Mediated Growth Method. *Chem. Mater.* **2003**, *15* (10), 1957−1962.
(25) Gou, L.; Murphy, C. J. Fine-Tuning the Shape of Gold Nanorods. *Chem. Mater.* **2005**, *17* (14), 3668−3672.
(26) Ye, X.; Gao, Y.; Chen, J.; Reifsnyder, D. C.; Zheng, C.; Murray, C. B. Seeded Growth of Monodisperse Gold Nanorods Using Bromide-Free Surfactant Mixtures. *Nano Lett.* **2013**, *13* (5), 2163−2171.
(27) Lin, W. K.; Cui, G.; Burns, Z.; Zhao, X.; Liu, Y.; Zhang, Z.; Wang, Y.; Ye, X.; Park, Y.; Lee, S. E. Optically and Structurally Stabilized Plasmo-Bio Interlinking Networks. *Adv. Mater. Interfaces* **2021**, *8*, 2001370.
(28) Lee, S. E.; Liu, G. L.; Kim, F.; Lee, L. P. Remote Optical Switch for Localized and Selective Control of Gene Interference. *Nano Lett.* **2009**, *9* (2), 562−570.
(29) Lee, S. E.; Sasaki, D. Y.; Perroud, T. D.; Yoo, D.; Patel, K. D.; Lee, L. P. Biologically Functional Cationic Phospholipid-Gold Nanoplasmonic Carriers of RNA. *J. Am. Chem. Soc.* **2009**, *131* (39), 14066−14074.
(30) Zijlstra, P.; Chon, J. W. M.; Gu, M. Five-Dimensional Optical Recording Mediated by Surface Plasmons in Gold Nanorods. *Nature* **2009**, *459* (7245), 410−413.
(31) Sönnichsen, C.; Reinhard, B. M.; Liphardt, J.; Alivisatos, A. P. A Molecular Ruler Based on Plasmon Coupling of Single Gold and Silver Nanoparticles. *Nat. Biotechnol.* **2005**, *23* (6), 741−745.
(32) Sönnichsen, C.; Franzl, T.; Wilk, T.; von Plessen, G.; Feldmann, J.; Wilson, O.; Mulvaney, P. Drastic Reduction of Plasmon Damping in Gold Nanorods. *Phys. Rev. Lett.* **2002**, *88* (7), 77402.
(33) Lee, S. E.; Liu, G. L.; Kim, F.; Lee, L. P. Remote Optical Switch for Localized and Selective Control of Gene Interference. *Nano Lett.* **2009**, *9* (2), 562−570.
(34) Lee, S. E.; Sasaki, D. Y.; Perroud, T. D.; Yoo, D.; Patel, K. D.; Lee, L. P. Biologically Functional Cationic Phospholipid-Gold Nanoplasmonic Carriers of RNA. *J. Am. Chem. Soc.* **2009**, *131* (39), 14066−14074.
(35) Lee, S. E.; Lee, L. P. Biomolecular Plasmonics for Quantitative Biology and Nanomedicine. *Curr. Opin Biotechnol* **2010**, *21* (4), 489−497.
(36) Lee, S. E.; Lee, L. P. Nanoplasmonic Gene Regulation. *Curr. Opin Chem. Biol.* **2010**, *14* (5), 623−633.
(37) Lee, S. E.; Sasaki, D. Y.; Park, Y.; Xu, R.; Brennan, J. S.; Bissell, M. J.; Lee, L. P. Photonic Gene Circuits by Optically Addressable SiRNA-Au Nanoantennas. *ACS Nano* **2012**, *6* (9), 7770−7780.
(38) Lee, S. E.; Alivisatos, A. P.; Bissell, M. J. Toward Plasmonics-Enabled Spatiotemporal Activity Patterns in Three-Dimensional Culture Models. *Systems Biomedicine* **2013**, *1* (1), 12−19.
(39) Lee, S. E.; Chen, Q.; Bhat, R.; Petkiewicz, S.; Smith, J. M.; Ferry, V. E.; Correia, A. L.; Alivisatos, A. P.; Bissell, M. J. Reversible Aptamer-Au Plasmon Rulers for Secreted Single Molecules. *Nano Lett.* **2015**, *15* (7), 4564−4570.
(40) Liu, Y.; Park, Y.; Lee, S. E. Thermo-Responsive Mechano-Optical Plasmonic Nano-Antenna. *Appl. Phys. Lett.* **2016**, *109* (1), 013109.
(41) Murphy, E.; Liu, Y.; Krueger, D.; Prasad, M.; Lee, S. E.; Park, Y. Visible-Light Induced Sustainable Water Treatment Using Plasmo-Semiconductor Nanogap Bridge Array, PNA. *Small* **2021**, *17*, 2006044.

https://doi.org/10.1021/acsanm.3c04361
ACS Appl. Nano Mater. XXXX, XXX, XXX−XXX

(42) Liu, Y.; Zhang, Z.; Park, Y.; Lee, S. E. Ultraprecision Imaging and Manipulation of Plasmonic Nanostructures by Integrated Nanoscopic Correction. *Small* **2021**, *17* (21), 1−8.
(43) Saha, T.; Mondal, J.; Khiste, S.; Lusic, H.; Hu, Z.-W.; Jayabalan, R.; Hodgetts, K.; Jang, H.; Sengupta, S.; Lee, S. E.; Park, Y.; Lee, L. P.; Goldman, A. Nanotherapeutic Approaches to Overcome Distinct Drug Resistance Barriers in Models of Breast Cancer. *Nanophotonics* **2021**, *10* (12), 3063−3073.
(44) Park, Y.; Yoon, H. J.; Lee, S. E.; Lee, L. P. Multifunctional Cellular Targeting, Molecular Delivery, and Imaging by Integrated Mesoporous-Silica with Optical Nanocrescent Antenna: MONA. *ACS Nano* **2022**, *16* (2), 2013−2023.
(45) Zhang, Z.; Jeong, H.; Zu, D.; Zhao, X.; Senaratne, P.; Filbin, J.; Silber, B.; Kang, S.; Gladstone, A.; Lau, M.; Cui, G.; Park, Y.; Lee, S. E. Dynamic Observations of CRISPR-Cas Target Recognition and Cleavage Heterogeneities. *Nanophotonics* **2022**, *11* (19), 4419−4425.
(46) Liu, Y.; Zu, D.; Zhang, Z.; Zhao, X.; Cui, G.; Hentschel, M.; Park, Y.; Lee, S. E. Rapid Depolarization-Free Nanoscopic Background Elimination of Cellular Metallic Nanoprobes. *Advanced Intelligent Systems* **2022**, *4*, 2200180.
(47) Do, H.; Yoon, C.; Liu, Y.; Zhao, X.; Gregg, J.; Da, A.; Park, Y.; Lee, S. E. Intelligent Fusion Imaging Photonics for Real-Time Lighting Obstructions. *Sensors* **2023**, *23*, 323.
(48) Krueger, D.; Graves, A.; Chu, Y.; Pan, J.; Lee, S. E.; Park, Y. Integrated Plasmonic Gold Nanoparticle Dimer Array for Sustainable Solar Water Disinfection. *ACS Appl. Nano Mater.* **2023**, *6* (7), 5568−5577.
(49) Da, A.; Chu, Y.; Krach, J.; Liu, Y.; Park, Y.; Lee, S. E. Optical Penetration of Shape-Controlled Metallic Nanosensors across Membrane Barriers. *Sensors* **2023**, *23*, 2824.
(50) Cui, G.; Liu, Y.; Zu, D.; Zhao, X.; Zhang, Z.; Kim, D.; Senaratne, P.; Fox, A.; Sept, D.; Park, Y.; Lee, S. E. Opening Long-Time Investigation Window by Nonbleaching Phase Intensity Nanoscope: PINE. *arXiv*; 2023, 2303.03344.
(51) Steves, M. A.; Knappenberger, K. L. Distinguishing Single-Metal Nanoparticles with Subdiffraction Spatial Resolution Using Variable-Polarization Fourier Transform Nonlinear Optical Microscopy. *Chemical & Biomedical Imaging* **2023**, *1* (1), 91−98.
(52) Li, Z.; Kang, L.; Lord, R. W.; Park, K.; Gillman, A.; Vaia, R. A.; Schaak, R. E.; Werner, D. H.; Knappenberger, K. L. Plasmon-Mediated Chiroptical Second Harmonic Generation from Seemingly Achiral Gold Nanorods. *ACS Nanoscience Au* **2022**, *2* (1), 32−39.
(53) Cui, G.; Kim, D. Y.; Zu, D.; Chai, G.; Lee, S. E. Resolving Proximal Nanometer Objects below the Diffraction Limit with Interferometric Phase Intensity Nanoscopy. *arXiv*; 2023, 2310.02158.
(54) Dietz, H.; Berkemeier, F.; Bertz, M.; Rief, M. Anisotropic Deformation Response of Single Protein Molecules. *Proc. Natl. Acad. Sci. U.S.A.* **2006**, *103*, 12724.
(55) Aitken, C. E.; Petrov, A.; Puglisi, J. D. Single Ribosome Dynamics and the Mechanism of Translation. *Annual Review of Biophysics* **2010**, *39*, 491−513.
(56) Dastjerdi, H. M.; Dahmardeh, M.; Gemeinhardt, A.; Gholami Mahmoodabadi, R.; Köstler, H.; Sandoghdar, V. Optimized Analysis for Sensitive Detection and Analysis of Single Proteins via Interferometric Scattering Microscopy. *J. Phys. D Appl. Phys.* **2022**, *55* (5), 054002.
(57) Dahmardeh, M.; Mirzaalian Dastjerdi, H.; Mazal, H.; Köstler, H.; Sandoghdar, V. Self-Supervised Machine Learning Pushes the Sensitivity Limit in Label-Free Detection of Single Proteins below 10 KDa. *Nat. Methods* **2023**, *20* (3), 442−447.

https://doi.org/10.1021/acsanm.3c04361
ACS Appl. Nano Mater. XXXX, XXX, XXX−XXX